Ability of the R3 test to evaluate differences in early age reactivity of 16 industrial ground granulated blast furnace slags (GGBS)

Simon Blotevogel, Andreas Ehrenberg, Laurent Steger, Lola Doussang, Judit Kaknics, Cédric Patapy, Martin Cyr

Ability of the R3 test to evaluate differences in early age reactivity of 16 industrial ground granulated blast furnace slags (GGBS)

Postprint version of the article published in Cement and Concrete Research under DOI:
10.1016/j.cemconres.2020.105998

Authors

Simon Blotevogel[1], Andreas Ehrenberg[2], Laurent Steger[1,3], Lola Doussang[3], Judit Kaknics[4], Cedric Patapy[1], Martin Cyr[1]

[1] *LMDC, Université de Toulouse, INSA/UPS Génie Civil, 135 Avenue de Rangueil, 31077, Toulouse cedex 04, France*
[2] *Institut Für Baustoff-Forschung EV (FEHS), Bliersheimer Str.62, Duisburg 47229, Germany*
[3] *Ecocem Materials, 324061, Block F1, Eastpoint Business Park, Dublin 3, Ireland*
[4] *ArcelorMittal Maizieres Research, Voie Romaine, 57283 Maizières-les-Metz, France*

Abstract

Ground granulated blast furnace slag (GGBS) is a glassy by-product of pig iron production and is commonly used in concrete industry to replace cement and thereby lower the carbon footprint of the material. Large variations in reactivity exist depending on the GGBS physical and chemical features. Here we investigate the ability of three rapid calorimetric methods to evaluate the reactivity of GGBS. On a set of 16 industrial GGBS, we show that 24h heat release, using the R3-protocol, correlates well with 2d compressive strength of standard mortars using 75 wt.-% GGBS. The correlation of R3-test results (R^2= 0.87) is better than for traditional reactivity indices calculated from chemical composition. Furthermore, we present data on the repeatability of the test protocol and show that the R3 protocol is very sensitive to sample fineness. Finally, XRD patterns show that slight differences in phase assemblage exist between the most and least reactive GGBS.

1. Introduction

Ground granulated blast furnace slag (GGBS) is a glassy by-product of pig iron production and has been used in blended cements for over 140 years [1]. Besides economic aspects the use of GGBS at high substitution levels has the advantage of lowering CO_2 footprint of concrete, decreasing heat development during setting and increasing physical and chemical resistance of the material [1–6]. However, short term compressive strength development of GGBS is below that of original Portland cement (OPC), but reactivity under same conditions, can differ widely between different GGBS [1,4,7–10].

The intrinsic reactivity of GGBS depends on different parameters as chemical composition, glass content and structure or quenching parameters of the slag [1,9,11–13]. This makes modification of production parameters of GGBS – so called upstream modification - a promising route to increase its reactivity [13–15]. Another way to increase the reactivity of GGBS is the modification of the activation system (downstream) by increasing fineness, increasing reaction temperature, adapting solution chemistry or by adding chemical activators as $CaCl_2$ [16–18].

The present work originates in the European research project Actislag, aiming to develop a second generation GGBS reaching cement substitution rates of 80 wt.-% while keeping the specifications of CEM II. Therefore, both activation routes are considered: upstream modifications of GGBS chemistry/microstructure and downstream modifications of the activation system. In order to reach the research goals, it is essential to be able to quickly assess the reactivity of a large number of GGBS. Furthermore, as upstream modifications will be tested in lab scale trials, minimal sample mass should be used for the reactivity tests.

A multitude of test methods are available to predict the reactivity of supplementary cementitious materials (SCM). Usually chemical tests are used to predict short term compressive strength, see Snellings and Scrivener (2016) and Li et al. (2018) for a review [19,20]. Standardized test methods use

Ca consumption during hydration of the SCM (e.g. Chapelle test, Frattini test). These were designed for pozzolanic material and are difficult to apply to slags, as GGBS contain a substantial amount of reactive Ca [19]. Further methods aim to determine the degree of reaction of SCMs: most notably selective dissolution, SEM-IA, XRD, and NMR (27-Al or 29-Si) are presented in scientific literature but are often time consuming and with moderate accuracy at early age [21].

In recent publications heat development during hydration of a simplified system showed good correlation with compressive strength of different SCM containing mortars [19,20,22]. In these studies, a sulphate containing alkaline solution is added to a mix of portlandite, carbonates and the respective SCM. The heat development during the following reaction is measured by isothermal calorimetry. The reaction can be accelerated by increasing the temperature conditions. This setup avoids the use of other hydraulic material as OPC, and thus the risk of overprinting the signal of intrinsic SCM reactivity [23–25]. By this protocol a wide range of SCMs including GGBS, fly ash, natural pozzolans and calcined clays were tested and classified according to their reactivity. In Avet et al. (2016) the simplified test was used to predict the pozzolanic activity of 7 calcined clays, naming it R3 test [22]. In that study a good prediction of compressive strength of mortars containing 30 wt.-% calcined clays was obtained after 1d of calorimetric measurement at 40°C for all setting ages. Li et al. 2018 reached a good prediction of 28d compressive strength of mortars at a replacement rate of 30 wt.-% of cement by different SCMs. They used the same calorimetric test, but the best correlation between 28d compressive strength and heat development was reach for 3 and 7 d of calorimetric measures. Other studies used a similar test design to determine hydraulic or pozzolanic properties of different materials, including GGBS [26–28]. However, it was never attempted to use the R3 test to rank different GGBS according to their early age reactivity.

Another promising method to judge GGBS reactivity in literature is proposed by Kashani et al. (2014) [29]. In this study pure 1 molar NaOH is used as activation system which gives exploitable results in

73 less than 12 h in ambient temperature isothermal calorimetry, nevertheless no comparison between
74 different GGBS was attempted.

75 In the present study, 16 industrial GGBS from different sources were examined in terms of
76 composition and mechanical performance in binder pastes. Subsequently different calorimetric
77 protocols existing in literature were tested in order to develop a rapid and reliable method using
78 minimal sample mass to evaluate GGBS short term performance in cementitious systems. The three
79 main objectives of this study are:

80 1. Evaluation of existing calorimetric tests for the assessment of young age compressive
81 strength of GGBS. Main focus is on protocols based on the R3 test and the optimization of
82 grinding parameters.
83 2. Application of an optimized calorimetric test on a set of 16 industrial slags and comparison of
84 test results with actual compressive strength values in order to evaluate the capacity of the
85 test to evaluate the reactivity of different GGBS.
86 3. Discussion of sources of differences in reactivity of the analyzed GGBS, especially chemical
87 composition of the slags and mineral phases formed during the calorimetric test.

88

2. Materials

2.1 Chemical composition of industrial GGBS

In order to represent a wide range of today's GGBS compositions, 16 different slags were selected from the FEhS database (FEhS – Institut für Baustoff-Forschung e.V., Duisburg, Germany). Chemical composition was measured on fused tabs by XRF (Panalytical Zetium). The composition was calculated conventionally as oxides (Table 1). Major element compositions and maximum values from literature are displayed in Figure 1. CaO contents in our dataset are between 29.0 and 43.2 wt.-%. The lowest value is lower than lowest values reported in literature, but the highest value is also 4.3 wt.-% lower than maxima reported [1]. Most GGBS contain between 40 and 42 wt.-% CaO. SiO_2 contents in our GGBS set range from 34.6 to 39.2 wt.-%, a distribution that is on both ends about 2 % smaller than the extreme values for GGBS from different regions of the world reported in Matthes et al. (2018) [1]. For Al_2O_3 the observed concentrations range between 6.8 to 20.1 wt.-%, which corresponds to extreme values reported in literature [1]. However, only GGBS 15 attains such a high Al_2O_3 content (20.1 wt.-%), the next lower sample (GGBS 14) contains 13.7 wt.-% Al_2O_3. The majority of selected GGBS contain between 10 and 12 wt.-% Al_2O_3. MgO contents in our sample set are between 6.12 and 11.6 wt.-%, both extrema are 3 % below extreme values reported by Matthes et al (2018) [1]. In the studied GGBS, TiO_2 contents range for 0.27 to 3.02 wt.-%. With 3.02 wt.-% of TiO_2 in GGBS 9 the extreme values again correspond to the values observed by Matthes et al. (2018) [1]. In contrast, most GGBS contain between 0.5 and 1 wt.-% TiO_2. Reactivity indices were calculated according to the composition data.

Glass content of the 16 GGBS was measured by optical transmission light microscopy at FEhS. The sample was ground in an agate mortar and the 40-63 µm fraction was embedded in Canada balm. Then, glass content (in vol.-%) was measured on individual grains, using a lambda plate and polarisators 1000. The method is described in detail in Drissen (1994) [30]. Glass content of all slags was >99.8 vol.-%, only exceptions were GGBS 14 (98.2 vol.-%) and GGBS 15 (94.5 vol.-%).

Furthermore, XRD scans were performed on the unhydrated slags (Figure 2). The measurement parameters were the same as described in section 3.3. Rietveld refinement using rutile as external standard gave an amorphous content of 96.2 vol.-% and 3.8 vol.-% of Spinel in GGBS 15. This is well in line with glass content measurements. In GGBS 13, amorphous content 97.4 vol.-% and 2.6 vol.-% of akermanite were modelled, slightly more than expected from glass content measurements. In all other samples, the crystalline signal was too weak to be modelled by Rietveld refinement, in line with glass content measurements. However, traces of merwinite were detected in GGBS 4 and GGBS 16, and traces of akermanite in GGBS 1, GGBS 2, GGBS 11 and GGBS 16.

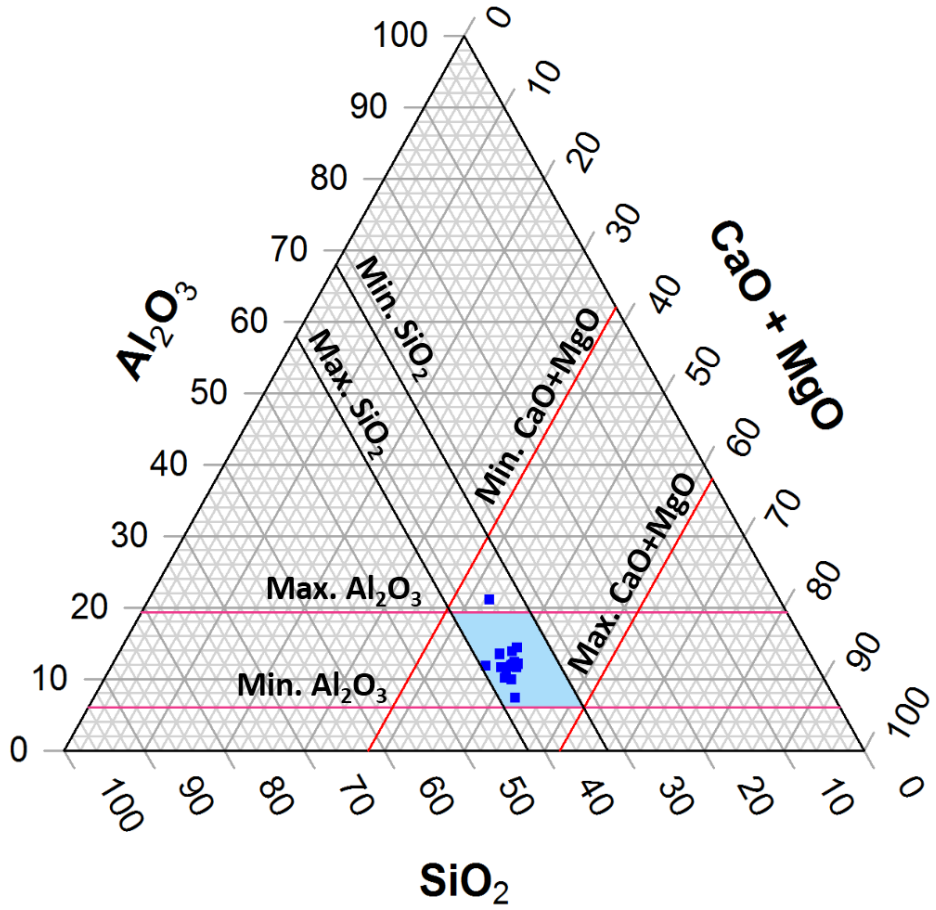

Figure 1. Major chemical composition of the 16 slags used in this study. The sum of concentration of the four presented elements was normalized to 100 wt.--%. Lines indicate minimum and

maximum contents reported in Matthes et al. (2018) [1]**. The blue patch indicates possible range of composition within those limits.**

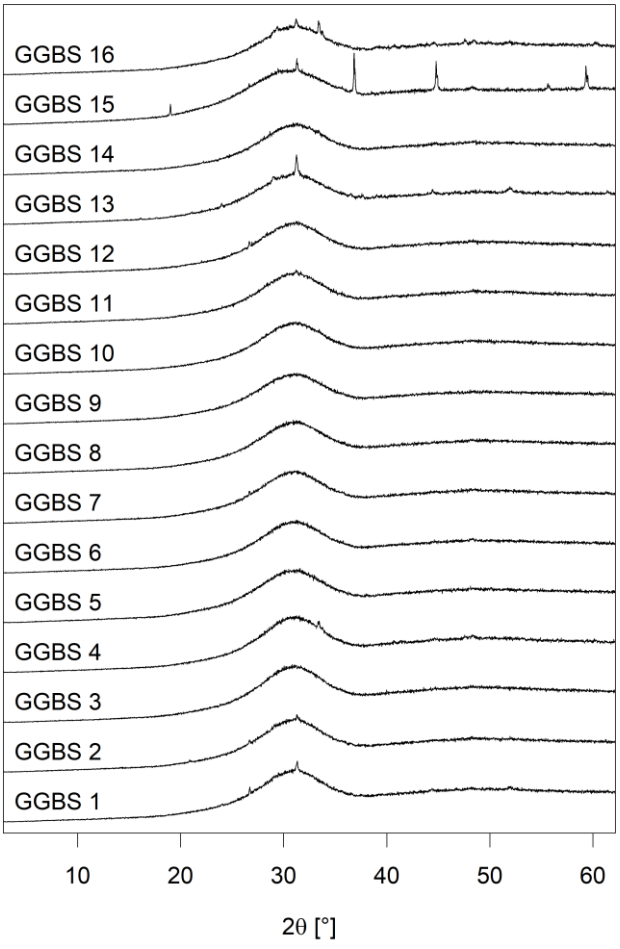

Figure 2. XRD scans of unhydrated GGBS. All GGBS have a high amorphous content. Crystalline phases were modelled for GGBS 15 and GGBS 13 using Rietveld refinement. GGBS 15 contains 3.8 vol.-% spinel and GGBS 13 2.6 vol.-% akermanite. For all other slags crystalline signal was too low to be modelled. However, traces of merwinite and/or akermanite were detected in GGBS 1, GGBS 2, GGBS 4, GGBS 11, GGBS 16.

Table 1. GGBS compositions as determined by XRF. Mean values and relative standard deviation (RSD, in %) are given for the measured parameters.

ID	CaO	SiO_2	Al_2O_3	MgO	TiO_2
	wt.-%	wt.-%	wt.-%	wt.-%	wt.-%
GGBS 1	41.4	36.4	13.6	6.80	0.75
GGBS 2	42.0	36.6	12.0	6.94	0.74
GGBS 3	40.9	37.6	9.61	6.40	0.61
GGBS 4	42.1	37.0	9.41	6.12	0.66
GGBS 5	38.4	37.1	12.9	7.32	0.77
GGBS 6	41.2	35.6	11.0	6.84	1.79
GGBS 7	41.7	36.7	11.5	6.35	0.70
GGBS 8	40.9	36.6	11.2	6.84	1.12
GGBS 9	39.5	37.4	11.0	6.64	3.02
GGBS 10	41.7	38.0	10.1	6.46	0.40
GGBS 11	43.2	36.3	11.8	6.30	0.43
GGBS 12	42.0	36.8	11.7	6.60	0.70
GGBS 13	33.9	39.2	11.2	10.4	0.57
GGBS 14	38.9	34.6	13.7	8.36	1.16
GGBS 15	29.0	34.6	20.1	11.6	0.78
GGBS 16	37.4	36.7	6.8	11.1	0.27
Mean	39.6	36.7	11.7	7.6	0.90
RSD (%)	9.2	3.1	23.9	23.9	73.8

2.2 Other Materials

The chemical composition of the clinker used for compressive strength tests is reported in Table 2. XRD analysis followed by Rietveld refinement gave a mineral composition of 60.9 wt.-% C3S, 21.5 wt.-% C2S, 0.9 wt.-% orthorhombic C3A, 7.8 wt.-% cubic C3A and 6.6 wt.-%C4AF. Density was 3.093 g/cm^3 and fineness 4200 cm^2/g (Blaine). Further reactants used were K_2SO_4 (VWR, REACTAPUR), KOH (VWR, AnalaR Normapur), $Ca(OH)_2$ (Merck, ACS Reagent, for analysis). Water used for calorimetric tests was always pure (18.2MΩ).

Table 2. Composition of the clinker used for compressive strength test and calorimetric tests. The values were determined by XRF.

Component	Content wt.-%
CaO	66.20
Free lime	0.64
MgO	1.00
SiO_2	22.10
Al_2O_3	5.20
Fe_2O_3	2.30
Mn_2O_3	<0.05
Cr_2O_3	<0.05
TiO_2	0.30
Na_2O	0.20
K_2O	0.74
S total	0.39
CO_2	0.07
H_2O	0.17

3. Methods

3.1 Compressive strength tests

Mortar strength tests according to EN 196-1 were performed in order to evaluate reactivity of GGBS [31]. A batch of 5 kg of each GGBS was ground in a ball mill using a mixture of steel spheres and cylinders. To achieve a fineness of about 4200 cm^2/g according to EN 196-6, the grinding time was about 3 hours [32]. However, the decisive parameter to evaluate the achieved fineness was the particle size distribution measured by laser diffraction granulometry (Horiba LA 300). Based on a weighted double logarithmic transformation according to the RRSB method, the PSD parameters d' ($d_{63.2\%}$) and n (slope) were calculated. For each sample, 6 standard prisms (4 x 4 x 16 cm^3) were made using 75 wt.-% of GGBS and 25 wt.-% of clinker according to EN 196-1, subsequently adding 4.5 wt.-% of SO_3, in form of a mixture of 25 wt.-% gypsum and 75 wt.-% anhydrite. A water binder ratio of 0.5 was used. Compressive strength tests were performed after 1d, 2d, 7d, 28d and 91d storing times at 20°C under water.

3.2 Isothermal Calorimetry

All calorimetric tests were carried out using a TAM Air isothermal calorimeter by TA-instruments. Samples were prepared in 10 mL polypropylene recipients. The pastes were hand stirred using a glass bar until no agglomerates or layering was visible anymore. Only exception was the 7d calorimetric test using clinker, based on EN196-9, for which samples were prepared in a 20 mL admixture cell [33]. Results of calorimetric measurements were normalized to GGBS mass in the vessel.

3.3 Characterization of hydrated phases

Hydrates were characterized directly after the calorimetric measurements. The hydrated slag sample was crushed in an agate mortar and the resulting powder was briefly suspended in a stirred beaker containing isopropanol to remove remaining water. The powder was then recovered through vacuum filtration and the sample was rinsed with acetone three times. Finally, the dry powder retained by

the filter was directly used for XRD analysis on a Brucker D8 using a Cu-cathode. Scan duration was 65 min for angles from 2 to 70°. The sample preparation from calorimeter to the start of XRD scan took less than 1h.

3.4 Method adaption for estimation of slag reactivity

In a first step, three modified, rapid test protocols from literature, described in Table 3, were tested for their capacity to predict compressive strength of slag-based mortars. The R3 protocol was modified in the sense that no calcite addition was used and the test proposed in Snellings and Scrivener 2016 was modified by reducing the amount of $Ca(OH)_2$ and not adding sulfates to the mix [19,20,22]. Therefore, six GGBS, covering a wide range of reactivity, were selected. Furthermore, heat development under the same conditions as the compressive strength tests (adding 25 wt.-% clinker, and anhydrite/gypsum to reach 4.5 wt.-% SO_3) was measured. For these tests, the same grinding protocol as for compressive strength tests was used.

Table 3. Summary rapid calorimetric tests take from literature and the standard test imitating conditions of the compressive strength measurements. Protocols were slightly modified to suit the needs of this study.

Protocol based on	liquid/solid ratio	Solid additions	Activation solution	Temperature	Duration
Kashani et al. 2014	0.45	-	0.5 M NaOH	20°C	20h
Avet et al. 2016 and Li et al.. 2018. **R3-Test**	1.25	$Ca(OH)_2$ (3:1) (addition : slag)	0.3 M K from KOH + K_2SO_4 (1 : 5 w/w)	40°C	24h
Snellings and Scrivener 2016	0.83	$Ca(OH)_2$ (2:1)	0.5 M KOH	40°C	24h
FEhS database for GGBS (75 wt.-% GGBS, 25 wt.-% CL [34]	0.50	Clinker/GGBS (1:3) 4.5 wt.-% SO_3	H_2O	20°C	7d

Next, the repeatability of the R3 protocol was tested measuring 7 times the same powder (GGBS 11) to calculate errors associated with the calorimetric method. Subsequently, the same granulate (GGBS 14) was ground six times and analyzed with the modified R3 test. Therefore, the samples were ground using a Retsch RS100 disc mill. 15 g of each GGBS was put in a 50 mL tungsten carbide bowl for 1 minute at 1400 rpm to a Blaine fineness of 4100 ± 100 cm^2/g [32].

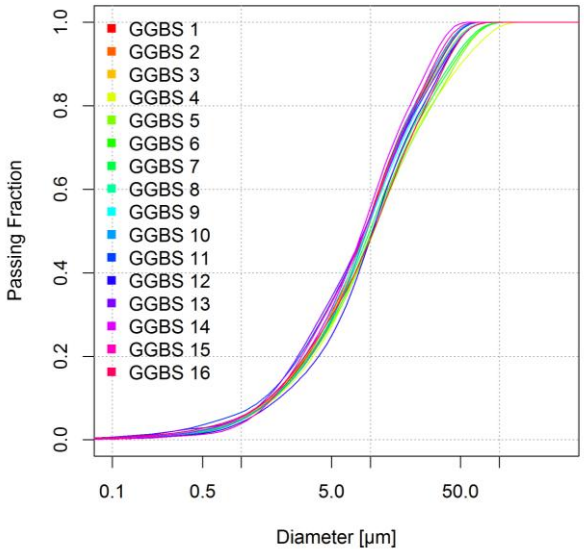

194

195 **Figure 3. Granulometric curves of 16 ground industrial GGBS samples, after applying the same**
196 **grinding protocol.**

197 As the repeatability of the whole protocol was judged sufficient, the grinding process and the R3
198 calorimetric measurements were applied to the set of 16 industrial GGBS. The particle size
199 distribution was measured on a CILAS 1090 laser diffraction granulometer operating with ethanol to
200 check repeatability of the grinding protocol (Figure 3). Three successive measurements in Fraunhofer
201 mode were carried out on each powder sample. Samples received 3x30 s ultrasonic treatment before
202 measurement in order to avoid agglomerations. The PSD analysis gave d_{10} values between 1.6 and
203 1.8 µm and d_{50} values between 8.5 and 10.5 µm. These values were judged sufficiently close to
204 exclude a major influence of sample finesse.

205 In addition, 50 g of GGBS 2 and GGBS 14 samples were ground for 2x30 s, 3x30 s, 4x30 s and 5x30 s in
206 the 250 mL bowl described above, in order to be able to quantify the impact of fineness on
207 calorimetric measurements.

208

4. Results

4.1 Chemical and mechanical analysis of GGBS

Mean compressive strength values are 2.8, 9.9, 30.7, 44.8 and 53.9 MPa at 1 d, 2 d, 7 d, 28 d and 91 d, respectively (Table 4). Measured compressive strength values logically increase with time for all samples. Compressive strength after 1 d is between 2.0 MPa in GGBS 9, the sample with the highest TiO_2 content, and 3.9 MPa in GGBS 2 and GGBS 11. This means a relative difference of almost a factor 2 in mechanical performance between different slags. Note that no compressive strength measurements are available for GGBS 15 and GGBS 16 at this age. After 2 d, measured values range from 3.7 (GGBS 16) to 17.1 MPa (GGBS 15), making up for difference of more than a factor 4 between the least and most reactive slag. These two are also the samples with the respectively lowest and highest Al_2O_3 contents (Table 1). The relative standard deviation (RSD) of compressive strength tests between samples increases to 38.4 % at 2 d time. RSD between samples then decreases over time (24.2 % after 7d and 14.3 % after 28 d) and is as low as 12.5 % after 91 d.

After 7 d, 28 d and 91 d time, GGBS 11 developed highest compressive strength (40.0, 54.3 and 62.4 MPa, respectively), this is also the sample with the highest CaO content (Table 1). This slag was already the most effective after 1 d when no data for GGBS 15 was available, but overtaken by GGBS 15 at 2 d. The relative performance of GGBS 15, the sample with the highest Al_2O_3 content and the lowest CaO content decreased over time. GGBS 16 continued to be the least reactive slag (12.0, 26.5 and 32.7 MPa, respectively). Note that the relative difference between the most and least reactive GGBS decreased at later ages. Between the extreme values, several slags interchanged their ranks at 7d, 28 d and 91 d, so that no clear tendency was visible. At 91 d all GGBS have reached compressive strength values of >50 MPa, with only two exceptions (GGBS 15 and GGBS 16).

Table 4. Results of compressive strength tests on mortar (75 wt.-% GGBS: 25 wt.-% Clinker). Mean values and relative standard deviation (RSD, in %) of 6 mortar bar specimens are given for all parameters.

ID	1 d	2 d	7 d	28 d	91 d
	MPa	MPa	MPa	MPa	MPa
GGBS 1	3.1	11.0	33.8	44.6	55.3
GGBS 2	3.9	11.2	37.3	47.5	56.7
GGBS 3	2.6	8.2	32.3	48.5	55.6
GGBS 4	2.8	9.4	32.4	48.9	57.3
GGBS 5	2.7	9.2	32.2	45.5	55.6
GGBS 6	2.4	9.2	28.1	45.5	54.9
GGBS 7	2.8	11.2	34.8	44.4	54.9
GGBS 8	2.1	10.3	31.4	43.8	51.8
GGBS 9	2.0	4.3	18.0	37.9	53.6
GGBS 10	2.5	7.4	32.7	46.3	51.2
GGBS 11	3.9	15.6	40.0	54.3	62.4
GGBS 12	3.1	10.6	39.2	50.6	57.7
GGBS 13	2.2	5.1	23.4	44.6	57.2
GGBS 14	3.0	14.8	35.1	49.2	59.4
GGBS 15	-	17.1	29.3	38.2	46.1
GGBS 16	-	3.7	12.0	26.5	32.7
Mean	2.8	9.9	30.7	44.8	53.9
RSD (%)	20.9	38.4	24.2	14.3	12.5

4.2 Reactivity indices

Reactivity indices are routinely used to evaluate GGBS quality. For the set of 16 industrial GGBS, different reactivity indices were calculated based on oxide contents of GGBS (Table 1), using formulas commonly found in literature (see Matthes et al., 2018, for discussion and initial sources [1]). Only the F-value by Ehrenberg (2015) was added [35]. Correlation coefficients (Pearson's R^2) between index values and measured compressive strength are given in Table 5. Most reactivity indices do not explain more than a third of the variance ($R^2<0.33$) observed in actual compressive strength measurements. Only the German standard for special cement, the basicity by Schwiete, the F-value by Keil and the F-value by Ehrenberg explain higher proportions of variance in compressive strength tests at some ages. Strongest correlations are found for 2 d compressive strength for the F-value by Keil ($R^2=0.71$), and Ehrenberg ($R^2=0.71$) and the German standard for special cement ($R^2=0.78$). At

younger and older ages, correlations are less well defined. Only the basicity by Schwiete gives stronger correlations at 7d (R^2=0.63) then after 2d (R^2=0.51). The Schwiete basicity never drops below a correlation coefficient of 0.33 with R^2 of 0.41, 0.39 and 0.33 for 1 d, 28 d and 91 d, respectively. The Keil F-value also correlates well to 7 d compressive strength (R^2=0.43) but for all other ages drops below R^2 = 0.33. The F-value according to Ehrenberg correlates well with 1 d and 7 d strength (R^2 of 0.56 and 0.66 respectively) and the German standard for special cement only correlates with 1 d compressive strength (R^2=0.37).

Table 5. Pearson's R^2 of correlation between compressive strength at different mortar ages and reactivity coefficients calculated based on GGBS composition. Linear regression was carried out on all 16 GGBS characterized in this study except for the age of 1 d where the 14 first slags were used. Reactivity indices are taken from Ehrenberg (2015) and Matthes et al., (2018), original sources are cited therein [1,35]**.**

Reactivity index	Definition	1 d	2 d	7 d	28 d	91 d
Basicity according to Tetmajer	$\frac{C}{S}$	0.30	0.02	0.27	0.26	0.18
European Standard for slag cement (1994)	$\frac{(C+M)}{S}$	0.32	0.11	0.15	0.09	0.04
German Standard for special cement (1942)	$\frac{(C+M+A)}{S}$	0.37	0.78	0.31	0.08	0.05
German Standard for Eisenportlandzement (1909)	$\frac{(C+M)}{(S+A)}$	0.15	0.13	0.00	0.00	0.01
German Standard for Hochofenzement (1932)	$\frac{(C+M+\frac{1}{3}A)}{(S+\frac{2}{3}A)}$	0.29	0.01	0.03	0.02	0.00
Basicity by Schwiete	$\frac{(C+A-10)}{(S+10)}$	0.41	0.51	0.63	0.39	0.33
F-Value according to Keil (1942)	$\frac{(C+\frac{1}{2}M+\frac{1}{2}S^{2-}+A)}{(S+MnO)}$	0.36	0.65	0.48	0.21	0.16

F-Value according Ehrenberg (2015)	$\frac{(C+\frac{1}{2}M+\frac{1}{2}S^{2-}+A)}{(S+MnO+(TiO_2)^2)}$	0.56	0.71	0.66	0.26	0.09

259

260 **4.3 Correlating heat of hydration to compressive strength**

261 **4.3.1 Choice of the method**

262 The results of heat measurement of 6 selected slags using different methods are reported in Table 6.
263 Note that heat values are normalized to slag mass in the measurement vessel. For all three rapid test
264 methods the ranking of samples by heat development is similar. GGBS 13 is developing the least heat
265 whereas GGBS 14 shows the most exothermic reaction. Only in the method by Kashani et al. (2014),
266 without Ca addition, the lowest heat development is measured in GGBS 3 [29]. The methods taken
267 from Snellings and Scrivener (2016) and the R3 test gave the same ranking and similar magnitudes of
268 heat development [19,20,22]. However, the range of measured values is slightly larger in the R3-test
269 (between 187 and 303 J/g) than in the protocol taken from Snellings and Scrivener (between 184 and
270 257 J/g). Divided by their respective mean heat values this gives a relative span of 47 % for the R3
271 test and 31 % for the Scrivener and Snellings (2016) protocol, showing that the R3-test has a better
272 discriminatory capacity. Heat development per mass GGBS is lowest in the teste taken from Kashani
273 et al. (2014). The range of the measured values between 35.5 and 43.8 J/g is low, even considering
274 the low average heat of 40.1 J/g (relative span, 21 % of the mean). In the method imitating
275 compressive strength test by clinker addition, GGBS 11 has the highest heat development and GGBS
276 13 the least. The range of the data relatively close, between 308 and 366 J/g for an average of 335
277 J/g (17 % of the mean), giving the test lowest discriminatory capacity of the four tested methods.

278

279

280

Table 6. Heat development of six selected slags measured by different protocols together with Pearson's R^2 of linear regressions between heat and compressive strength for various curing times. Heat values are normalized to slag mass in the vessel.

Kashani et al. 2014		Modified Snellings and Scrivener 2016		R3, Avet et al. 2016, Li et al. 2018		7 d using clinker as compressive strength test	
Slag ID	**Heat 20h** [J/g]	**Slag ID**	**Heat 24h** [J/g]	**Slag ID**	**Heat 24h** [J/g]	**Slag ID**	**Heat 7d** [J/g]
GGBS 2	42.8	**GGBS 2**	240	**GGBS 2**	246	**GGBS 2**	337
GGBS 3	35.5	**GGBS 3**	218	**GGBS 3**	220	**GGBS 3**	340
GGBS 11	42.4	**GGBS 11**	250	**GGBS 11**	287	**GGBS 11**	366
GGBS 12	39.1	**GGBS 12**	230	**GGBS 12**	232	**GGBS 12**	322
GGBS 13	37.5	**GGBS 13**	184	**GGBS 13**	187	**GGBS 13**	308
GGBS 14	43.2	**GGBS 14**	257	**GGBS 14**	303	**GGBS 14**	335
		R^2 for linear regression between compressive strength and heat of hydration					
1 d	0.58	**1 d**	0.58	**1 d**	0.40	**1 d**	0.53
2 d	0.67	**2 d**	0.92	**2 d**	0.95	**2 d**	0.59
7 d	0.34	**7 d**	0.73	**7 d**	0.47	**7 d**	0.47
28 d	0.17	**28 d**	0.51	**28 d**	0.47	**28 d**	0.68
91 d	0.40	**91 d**	0.32	**91 d**	0.52	**91 d**	0.40

Linear regression of heat values against compressive strength for different ages, show similar patterns for the three rapid methods. Accuracy of fit is judged by Pearson's R^2 for linear regressions (Table 6). The best fit is achieved for 2 d resistance values for the three model systems. The best correlation is calculated between the R3 test heat and 2 d compressive strength with an R^2 of 0.95, followed by the method taken from Snellings and Scrivener (2016) with an R^2 of 0.92. These R^2 values are similar to the correlation coefficients observed for calcined clay reactivity and 28d compressive strength of various SCMs [19,22]. Goodness of fit is progressively degrading towards higher and lower ages.

294 Only the method taken from Kashani et al. 2014 shows a better fit for 91 d old samples than for 28 d
295 and 7 d old samples [29]. Generally, fits are less accurate for the Kashani et al. 2014 method,
296 between 0.67 and 0.17. In the 7 d method adding clinker, the distribution of Pearson's R^2 values
297 differs from the model systems [29]. In this method, best fit is calculated for 28 d strength (0.68) and
298 2 d strength (0.59). Surprisingly, the correlation coefficient for 7 d compressive strength
299 corresponding to the calorimetric measurement time of 7 d is less well (0.47). However, the
300 correlation coefficient is never as high as for the methods at 40°C and Ca excess.

301 Heat curves of the Kashani et al. (2014) method (Figure 4) show different curve shapes for different
302 samples, with for example heat development of GGBS 13 starting after about 7 h and then starting to
303 overtake all other slags from 20 h on, also other heat curves intersect [29]. Also in the 7d test
304 method and the R3 test some sample change ranks during the test. This makes the cutoff time a
305 relevant parameter in the testing process. In literature, different cutoff times were proposed for the
306 R3 test. In Avet et al. (2016), 1 d measurements correlated well with compressive strength
307 development of blended cements containing calcined clays at all ages. Independent of SCM type it
308 was found that 3 d and 7 d heat release by the R3 test correlated well with 28 d compressive
309 strength of 30 % SCM blended cements, for various SCMs. 7 d compressive strength was well
310 correlated with all tested calorimetric cutoff times (0.5, 1, 3 and 7 d).

311 The R3-test was retained for further investigation for its large span of heat values, best correlation
312 with 2 d compressive strength results and its easier sample handling due to high water content.

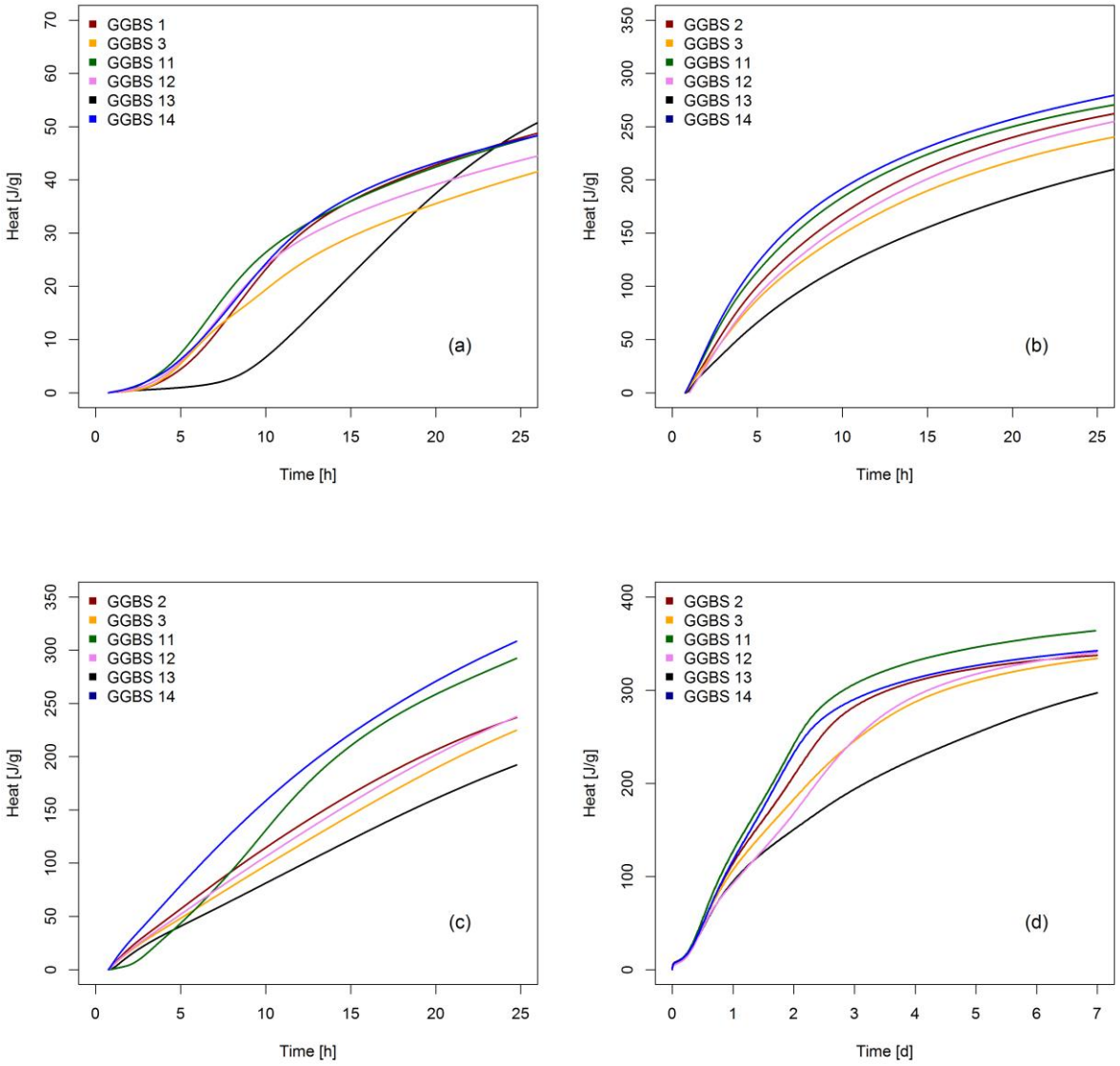

313

314 **Figure 4. Isothermal calorimetry results applying the four different methods to 6 selected GGBS.**
315 **(a) Method described by Kashani et al. (2014)**[29]**, (b) method by Snellings and Scrivener (2016)**
316 [20]**, (c) R3 test described by Avet et al. (2016) and Li et al. (2018)** [19,22] **and (d) calorimetric test**
317 **using GGBS/clinker mixture (75:25) and sulfates according to EN 196-1** [31]**. Note the different time**
318 **scale for (d). All heat measurements are normalized to slag mass in the vessel.**

319

320

4.3.2 Method validation and sample preparation

Validation of the R3 protocol showed good repeatability with a relative standard deviation of 0.87 % of the mean value (Table 7). The relative standard deviation of the same granulate ground 6 times had a relative standard deviation of 1.59 %.

Table 7. Validation of the R3 protocol. The first sample set shows values measured on the same powder sample. In the second set grinding was included in the procedure.

Sample type	Same Powder		Same granulate	
	Sample	Heat [J/g]	Sample	Heat [J/g]
	GBS 11.1	294.05	GGBS 14.1	264.17
	GBS 11.2	292.76	GGBS 14.2	264.37
	GBS 11.3	299.53	GGBS 14.3	263.53
	GBS 11.4	297.52	GGBS 14.4	271.33
	GBS 11.5	293.86	GGBS 14.5	258.98
	GBS 11.6	292.91	GGBS 14.6	261.12
	GBS 11.7	294.04		
Mean [J/g]		294.95		263.92
SD [J/g]		2.56		4.18
Relative SD [%]		0.87		1.59

Measuring samples of different finesse point out the impact of specific surface on heat of hydration (Figure 5). The specific surface of the different samples was between 2500 ±100 and 4800 ±100 cm^2/g, as determined by the Blaine method [32]. As expected, a higher reaction heat was measured when the samples were finer. Linear regression of reaction heat on Blaine value gave R^2 values > 0.95, thus proportionality can be assumed. Applying the regression function suggests, that reaction heat increased by about 4 J/g for each 100 cm^2/g increase of reactive surface.

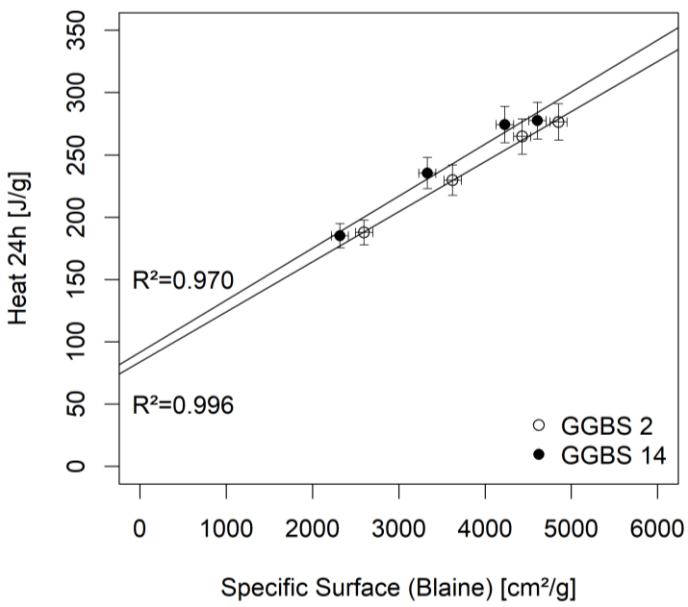

334

335 **Figure 5. Heat of hydration of GGBS 2 and GGBS 14 samples ground to different specific surface**
336 **values, using the modified R3 protocol. Vertical error bars correspond to 2RSD intervals as**
337 **described above. Horizontal error bars correspond to an average error of ±100 cm²/g for the Blaine**
338 **method.**

339

340 **4.3.3 Application of the R3-test on the set of 16 industrial GGBS**

341 In a last step all industrial slag samples were measured using the retained, R3 protocol. GGBS 9 was
342 the industrial slag with lowest heat development (144 J/g), whereas GGBS 15 showed highest
343 reaction heat with 319 J/g. The heat development for the 16 slag samples correlates well with mortar
344 compressive strength after 2 days (Table 4), as linear regression gave a R^2 of 0.87 (Figure 6). This
345 correlation coefficient is higher than for any reactivity index. The method error was estimated to be
346 3.2 % using the 2 RSD interval computed from the validation trial reported in Table 6. Taking into
347 account this error, not all slags can be separated from each other but there is a clear tendency for
348 higher heat values in more reactive slags.

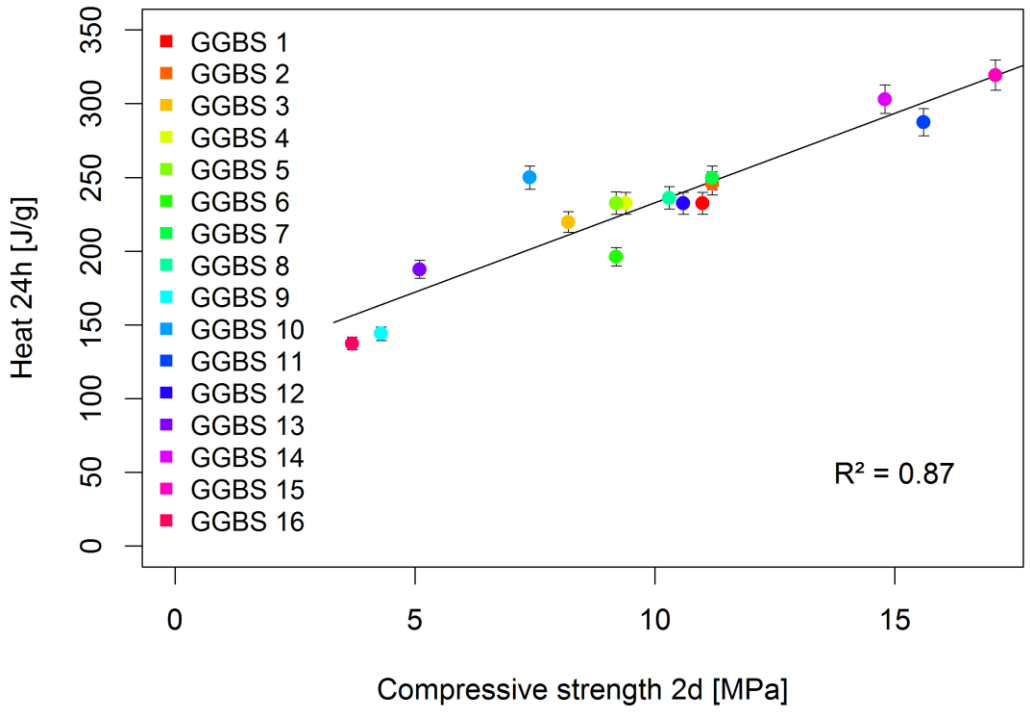

Figure 6. Heat of hydration of the whole set of 16 GGBS, plotted against 2d compressive strength test results. Vertical error bars correspond to 2RSD intervals as described above.

4.4 Characterization of hydrates after calorimetric test

After 24 h reaction time portlandite is still the major mineral phase in all samples as can be seen from the intense reflection at 18° in Figure 7. Besides, similar crystalline (ettringite, kuzelite) and amorphous phases (hydrotalcite) can be identified on XRD spectra in all slags after running the R3 calorimetric measurements (Figure 7). However, marked differences exist in peak intensity. The kuzelite peaks are more intense in the most reactive slags, whereas ettringite peaks are virtually absent in those GGBS. In moderately reactive slags kuzelite, a monosulphate ($Ca_4Al_2(SO_4)(OH)_{12} \bullet 6$ H2O) and ettringite ($Ca_6Al_2(SO_4)_3(OH)_{12} \bullet 26\ H_2O$) peaks coexist, whereas ettringite peaks are much more pronounced in least reactive slags. A broad hydrotalcite peak is visible in all slags, but most pronounced in the most reactive slag GGBS 15. The broad peak shape is likely due to variable compositions and especially in Mg/Al ratios of hydrotalcite. Also, hydrotalcite peaks overlap with

364 those of monocarboaluminates. Even though source of carbonates are limited in our setting, both

365 phases might be present.

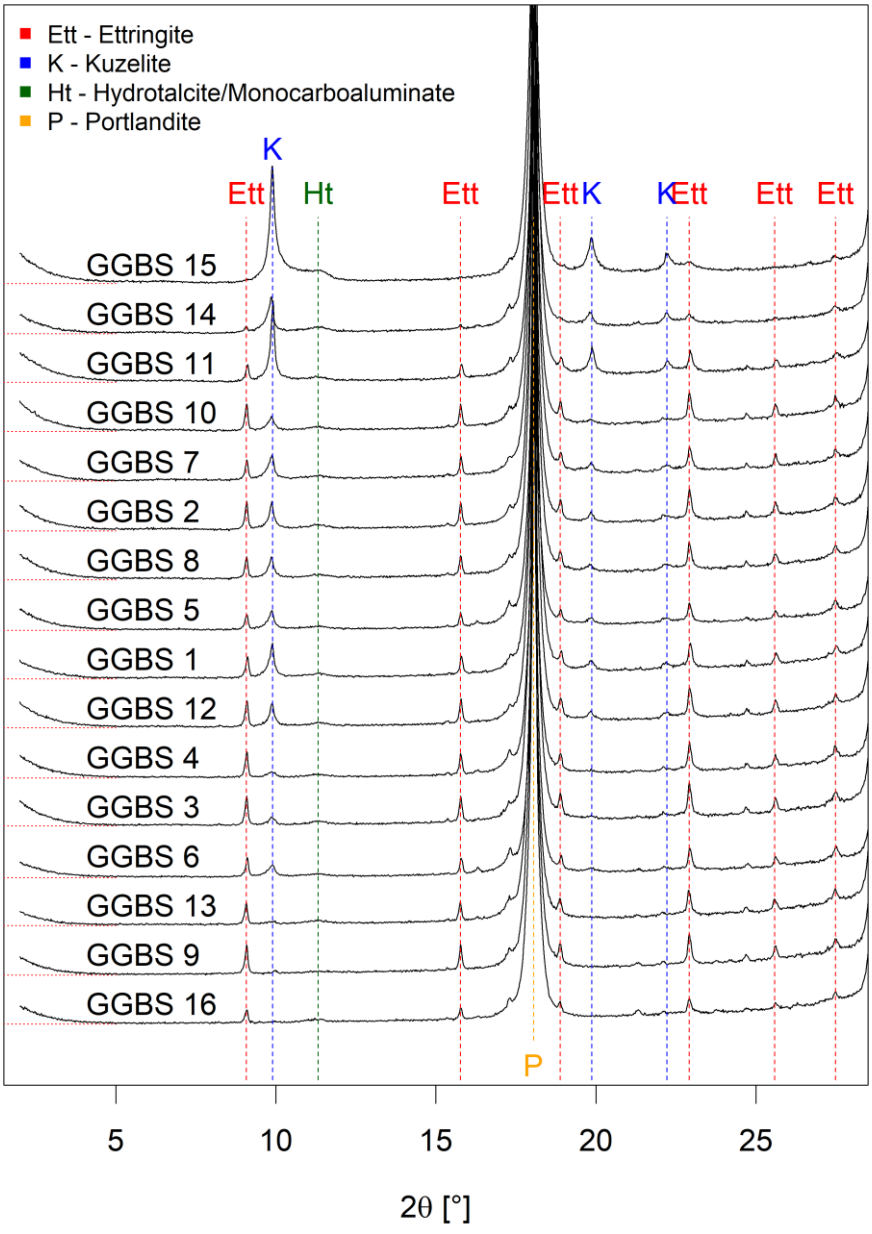

366

367 **Figure 7. XRD patterns of pastes hydrated for 24 h using R3 protocol. The slags are ordered**

368 **according to their 24h heat development (GBS 15 being the highest and GGBS 16 the least reactive**

369 **slag).**

370

371

5. Discussion

5.1 Differences in performance between different GGBS

Important differences in strength development were observed for the different slags. Compressive strength results at different hydration ages can differ by as much as a factor 4 between different slags (Table 4). The highest dispersion of compressive strength is observed for the 2 d time step, indicating a maximal influence of GGBS properties on compressive strength at this age. The highest dispersion and largest span make the 2 d time step the most relevant for reactivity testing, besides the practical interest in a short-term reactivity test.

At earlier ages, a major influence of clinker added is expected, due to its higher reaction rate [36]. At later ages, compressive strength values of different GGBS samples converge. In literature GGBS blended cements are known for ongoing hydration processes for long periods of time, also differences in reaction degree were still visible after 1 year [37]. This is consistent with the observation that strength development goes on until 91 d in our study, furthermore hierarchy between most and least reactive slags stay the same indicating that some influence of GGBS composition is still visible.

The exception is GGBS 15 with an extreme Al_2O_3 content. This sample shows the highest compressive strength at 2 d but performs less well at later ages (Table 4). Similar behavior is known for slags with high Al_2O_3 contents [9,10,38,39]. In blended cements, increased Al_2O_3 content of GGBS was reported to enhance reaction heat and early age strength [37,38]. This is in contrast to results obtained for alkali activated GGBS and activation systems using waterglass, where high Al_2O_3 contents had no or a negative effect on compressive strength [40,41]. In our case, the lower long-term compressive strength of GGBS 15 appears to be due to the low CaO content (Table 1). The CaO content of GGBS is reported to control short range order of C-S-H in alkali activated materials [42].

These observations underline the importance of Al-bearing phases for early age compressive strength, and the importance of C-S-H phases for later strength development.

Several reactivity indices correlate well with early age strength, all of them use CaO and Al_2O_3 as numerator (Table 5). Three of four also add MgO content as an asset. All divide by the SiO_2 content. This homogeneity underlines that the first order influence of those elements on GGBS reactivity is well understood. It is interesting to note that the index with the highest correlation with 2 d strength ((C+A+M)/S) can be approximated as (100-S)/S, thus the reactivity can be resumed only by the SiO_2 content of the slag [9]. All indices perform less well at later ages, underlining that strength development is less influenced by GGBS composition and reactivity at that stage. In the past Smolczyk 1978, used the same linear regression approach on a set on 196 GGBS, his regressions on 2 d compressive strength in mortar systems gave lower R^2 values [10]. This is likely due to higher and more stable glass contents and better control of minor elements in modern GGBS. Still, this underlines the importance of composition for GGBS reactivity.

The mechanisms of influences of composition on GGBS reactivity are multiple. The chemical composition of liquid slag exerts a control on the formation of the glass network. The higher the content of network modifiers Mg, Ca, Na, K, the lower is the polymerization degree of the glass network resulting in a less stable slag, showing higher dissolution rates [43,44]. Higher dissolution rates imply a quicker liberation of ions to the liquid phase, which precipitate to give secondary minerals that may develop material strength. The role of other elements in glass stability is less clear, Al and Ti for example can act as both network formers and modifiers. NMR studies on GGBS indicate mainly 4-coordinated Al, indicating rather a network former role of Al [38,45].

However, GGBS composition is not the only factor controlling glass structure. Also physical parameters of the production process influence the glass structure, most importantly thermal history, determined mainly by tapping temperature and quenching speed [1,11,14,15,46]. The presence of different elements in the glass network also modifies the dissolution of the glass, the

presence of network forming Al, for example increases the dissolution rate, as Al-O-Si sites are more easily attacked at high pH values than Si-O-Si groups [43]. In contrast, the insertion of other network formers like Zr slows down dissolution rates [47].

Chemical composition of GGBS also controls the element release into solution, as a congruent slag dissolution is expected [48,49]. Different stoichiometric ratios of elements can cause the formation of different secondary phases, as was observed in literature by XRD, SEM, DTG techniques and thermodynamic modelling of hydrated blended cements, and confirmed by XRD in this study [37]. For example MgO is essential for the formation of hydrotalcite like phases, and its formation lowers the uptake of Al in C-A-S-H phases [39,50]. Also, in alkali activated binders higher MgO content was found to increase reactivity (Ben Haha et al., 2011) [50]. Durdzinski et al. (2017) argue that the type of hydrates is not important for strength development in blended cements and that the key factor is space filling [51]. In contrast, Thermkhajorkit et al. 2014 found that in OPC pastes C-S-H phases are more important in compressive strength development than other hydrates [52].

The multitude of mechanisms by that GGBS composition influence its reactivity make clear that a prediction of reactivity only based on differences in composition is complex. Even though, differences in composition might be the reason for differences in reactivity. Furthermore structural and physical properties of the slag are neglected, calling for a more integrative method for evaluating reactivity [9].

5.2 Probing into reactivity using isothermal calorimetry

In the first test using 6 selected GGBS, the two protocols using $Ca(OH)_2$ addition at 40°C showed the best correlation with 2 d compressive strength values (Table 6). We chose the R3 method based on Avet et al., (2016) and Li et al., (2018) for further investigation as sample handling was much easier

443 due to higher l/s ratio and for higher absolute heat values and larger relative differences between
444 samples [19,22].

445 Applied to the set of 16 industrial GGBS, the R3 test gives better correlation with 2 d compressive
446 strength (R^2=0.87) in a 75 wt.-% GBGBS 25 wt.-% clinker system, than any of the reactivity indices
447 (Figure 6). Similar reaction pathways in the different samples can be assumed as heat curve shapes
448 are similar, only GGBS 11 shows a latency phase (Figure 4). The R3 test thus gives an intrinsic
449 reactivity of a given GGBS. This is especially interesting, as for the test no cement was used and thus
450 it gives comparable results of GGBS reactivity, without bias associated to the use of cement whose
451 composition might vary over time and with geographical origin. At later ages the test results
452 correlate less with compressive strength values, this in contrast to results obtained when calcined
453 clays were tested and heat release correlated well at all ages [22]. The test method, taken from
454 Snellings and Scrivener (2016), that also adds $Ca(OH)_2$ in excess, performed only slightly less well. The
455 similarity between the results indicate that Ca excess is crucial for the performance of the
456 calorimetric test. Li et al. (2019) reported that longer calorimetric measurement times (3d, 7d)
457 correlated well with 28 d compressive strength in a large variety of SCMs. In this study, however,
458 measurement of these time steps was not attempted.

459 The R3 test showed a high sensibility to sample finesse. When the test was performed on samples
460 ground to different finesses in the range of 2500 to 5000 cm^2/g the reaction heat increased
461 proportional to sample fineness (Figure 5). Applying the regression equation shows that in our case
462 heat release increases by about 4 J/g with every additional 100 cm^2/g of fineness. This is a great
463 advantage over chemical reactivity indices, as the important physical reactivity parameter – fineness,
464 is included in the measurement. On the other hand, when differences due to sample compositions
465 are to be assessed, one needs to take care to control for sample fineness. Superposing PSD curves
466 (Figure 3) of the 16 GGBS used in this study suggest that it is sufficient to apply the same grinding
467 protocol to obtain similar PSD in a wide range of GGBS. However, during method validation the RSD

between replicates increased to 1.59 % when grinding was included in the procedure (Table 7). When only the calorimetric protocol was repeated, the RSD was 0.87 %. This illustrates that the calorimetric protocol of the R3 test is repeatable and very sensitive even to slight changes in PSD.

The calorimetric test proposed by Kasahni et al., (2014) did not correlate as well with compressive strength, in the set of 6 GGBS [29]. This is likely due to the absence of a supplementary Ca-source in this test. It still showed highest correlation with compressive strength at 2 d (R^2 = 0.67). Different heat curve shapes indicate that the reaction mechanisms differed between different samples. This led to different rankings of GGBS at different time steps. It is interesting to note the high performance of GGBS 13 in this test. In the other tests, GGBS 13 was the least reactive slag. This finding indicates, that different GGBS might show different reactivities in different activation systems. This means that a badly performing GGBS with one system might show higher reactivity with another activation system. The differences in heat development indicate that GGBS composition has an impact on reactivity also in purely alkali activated systems. This is in contrast to earlier studies by Ben Haha et al., (2011 and 2012), yet we do not provide data on compressive strength of alkali activated materials [40,50].

Calorimetric measurements over 7 d, using the same clinker as the compressive strength test correlated less well with compressive strength results, than the formerly mentioned test at any time. It is especially interesting to note that also the 7 d compressive strength results, corresponding to the duration of the calorimetric measurements, only showed weak correlation with released heat.

5.3 Microstructure of samples and reaction mechanisms during the R3 test

XRD scans after the R3-test show similar phase assemblages in all samples. The detected phases are typically found in binders with high GGBS content, even though no cement was added [37]. However, Ca is supplied by portlandite excess and the concentrations of SO_4 and K mainly come from the

492 solution and are thus the same in all samples. There appears to be a systematic difference in
493 ettringite and AFm phases close to kuzelite structure. The XRD scans from least reactive GGBS show
494 no kuzelite peak, but a clearly distinguishable ettringite peak (Figure 7). For more reactive GGBS an
495 AFm peak close to kuzelite structure appears and its intensity overtakes that of ettringite for the
496 most reactive samples. In GGBS 15, the most reactive GGBS, no ettringite is detected. It is likely that
497 the higher Al content of the more reactive GGBS causes this shift, as a main difference between
498 those minerals is the Al/Ca ratio, with kuzelite containing more Al with respect to Ca, than ettringite.
499 This is consistent with former research showing that composition of hydrates can be modified by
500 GGBS compositions and high Al contents are good for early age strength development of GGBS [37].
501 The early strength development due to higher Al contents is often associated with voluminous
502 ettringite formation, this is not confirmed here [40,53]. Also, hydrotalcite appears to be more
503 abundant in the most reactive samples. Liberation of MgO from the GGBS is essential for the
504 formation of hydrotalcite like phases, and its formation lowers the uptake of Al in C-A-S-H phases
505 [39,50]. In alkali activated GGBS presence of hydrotalcite led to higher long-term compressive
506 strength due to reduced coarse pore volume [50]. Consequently, the formation of hydrotalcite
507 appears to be a desirable feature also in blends adding OPC or portlandite.

508 The importance of Al bearing hydrates for early age strength development might also be the reason
509 for the sensitivity of the R3-test to early age reactivity. Formation of Al bearing phases is very
510 exothermic, compared to the formation of C-S-H phases that are responsible for later age strength
511 [54]. Ettringite for example has a formation enthalpy of −17,535 kJ/mol under standard conditions,
512 whereas formation enthalpy of tobermorite is given with -1,916 kJ/mol, almost ten times less [54]. It
513 was argued that differences in hydration enthalpy are due to differences in the amount of water
514 integrated to the crystal structure [55]. Ettringite and AFm phase take up more water to their
515 structure than CSH phases and have higher molar volume [54,55]. The higher molar volume might
516 explain their importance in early age strength as these phases can rapidly fill up pore space. The
517 differences in formation enthalpies and molar volume could be the reason why the 7 d calorimetric

518 test does not correlate well with 7 d compressive strength. At this age, strength development might
519 not be controlled by the same phases that control heat release. A calorimetric test can only work
520 when both coincide, which appears to be the case for early age, in blended cements that contain
521 high proportions of GGBS.

6. Conclusion

1. Large difference in slag reactivity exist, those are mainly but not exclusively due to differences in GGBS composition. The influence is either due to dissolution rate of the glass or type and structure of hydrates formed.
2. Differences in 2 d strength of blended cement pastes can be conveniently predicted by the R3 method. The method does not work as well for later ages.
3. The R3 test proved to be highly sensitive to differences in fineness. Higher reactive surface yield higher reaction heat at a rate of approximately 4 J/g per 100 cm^2. This is a great advantage over reactivity indices.
4. Differences in compressive strength between GGBS in cements with high replacement rates are most pronounced at early age, most notably 2 d in the studied systems. This is likely due to the importance of Al bearing phases for early age strength.

Acknowledgements

This project has received funding from the Research Fund for Coal and Steel under grant agreement No 749809.

Bibliography

[1] W. Matthes, A. Vollpracht, Y. Villagrán, S. Kamali-Bernard, D. Hooton, E. Gruyaert, M. Soutsos, N. De Belie, Ground Granulated Blast-Furnace Slag, in: N. De Belie, M. Soutsos, E. Gruyaert (Eds.), Prop. Fresh Hardened Concr. Contain. Suppl. Cem. Mater., Springer International Publishing, Cham, 2018: pp. 1–53. https://doi.org/10.1007/978-3-319-70606-1_1.

[2] J. Bijen, Benefits of slag and fly ash, Constr. Build. Mater. 10 (1996) 309–314. https://doi.org/10.1016/0950-0618(95)00014-3.

[3] A. Ehrenberg, CO2 emissions and energy consumption of granulated blastfurnace slag, in: Proc. Manuf. Process. Iron Steel Slags, Euroslag publication, Keyworth, UK, 2002: pp. 151–166.

[4] F. Hogan, J. Meusel, Evaluation for Durability and Strength Development of a Ground Granulated Blast Furnace Slag, Cem. Concr. Aggreg. 3 (1981) 40. https://doi.org/10.1520/CCA10201J.

[5] H.F.W. Taylor, Cement chemistry, 2nd ed., Thomas Telford Publishing, 1997. https://doi.org/10.1680/cc.25929.

[6] P. Van den Heede, N. De Belie, Environmental impact and life cycle assessment (LCA) of traditional and 'green' concretes: Literature review and theoretical calculations, Cem. Concr. Compos. 34 (2012) 431–442. https://doi.org/10.1016/j.cemconcomp.2012.01.004.

[7] A. Ehrenberg, D. Israel, A. Kühn, HM. Ludwig, V. Tigges, W. Wassing, Hüttensand: Reaktionspotenzial und Herstellung optimierter Zemente Tl.1 (Granulated blast furnace slag: reaction potential and production of optimized cements, part 1), Cem. Int. (2008).

[8] N. Robeyst, E. Gruyaert, C.U. Grosse, N. De Belie, Monitoring the setting of concrete containing blast-furnace slag by measuring the ultrasonic p-wave velocity, Cem. Concr. Res. 38 (2008) 1169–1176. https://doi.org/10.1016/j.cemconres.2008.04.006.

[9] H.-G. Smolczyk, Structure des laitiers et hydratation des ciments de laitiers : structure et caractérisation des laitiers, in: Rapp. PRINCIPAUX, Paris, 1980: pp. III-1/1-1/17.

[10] H.-G. Smolczyk, Zum Einfluß der Chemie des Hüttensands auf die Festigkeit von Hochofenzementen, Zem. - Kalk - Gips. (1978) 294–296.

[11] N. Pronina, S. Krüger, H. Bornhöft, J. Deubener, A. Ehrenberg, Cooling history of a wet-granulated blast furnace slag (GBS), J. Non-Cryst. Solids. 499 (2018) 344–349. https://doi.org/10.1016/j.jnoncrysol.2018.07.054.

[12] F. Schröder, Slags and slag cements, in: Proc. 5th Int. Symp. Chem. Cem., Tokyo, 1969: pp. 149–199.

[13] R. Tänzer, A. Buchwald, D. Stephan, Effect of slag chemistry on the hydration of alkali-activated blast-furnace slag, Mater. Struct. 48 (2015) 629–641. https://doi.org/10.1617/s11527-014-0461-x.

[14] A. Ehrenberg, Influence of the granulation conditions and performance potential of granulated blast-furnace slag – Part 1: Granulation conditions, ZKG Int. (2013) 64–71.

[15] A. Ehrenberg, Influence of the granulation conditions and -performance potential of granulated blastfurnace slag – Part 2: Chemistry and physical properties, ZKG Int. (2013) 60–67.

[16] F. Bellmann, J. Stark, Activation of blast furnace slag by a new method, Cem. Concr. Res. 39 (2009) 644–650. https://doi.org/10.1016/j.cemconres.2009.05.012.

[17] K. Riding, D.A. Silva, K. Scrivener, Early age strength enhancement of blended cement systems by CaCl2 and diethanol-isopropanolamine, Cem. Concr. Res. 40 (2010) 935–946. https://doi.org/10.1016/j.cemconres.2010.01.008.

[18] L. Steger, C. Patapy, B. Salesses, M. Chaouche, M. Cyr, Acceleration of GGBS Cements by Chloride, New Insights on Early Hydration, (2017).

[19] X. Li, R. Snellings, M. Antoni, N.M. Alderete, M. Ben Haha, S. Bishnoi, Ö. Cizer, M. Cyr, K. De Weerdt, Y. Dhandapani, J. Duchesne, J. Haufe, D. Hooton, M. Juenger, S. Kamali-Bernard, S. Kramar, M. Marroccoli, A.M. Joseph, A. Parashar, C. Patapy, J.L. Provis, S. Sabio, M. Santhanam, L. Steger, T. Sui, A. Telesca, A. Vollpracht, F. Vargas, B. Walkley, F. Winnefeld, G. Ye, M. Zajac, S.

590 Zhang, K.L. Scrivener, Reactivity tests for supplementary cementitious materials: RILEM TC 267-
591 TRM phase 1, Mater. Struct. 51 (2018). https://doi.org/10.1617/s11527-018-1269-x.
592 [20] R. Snellings, K.L. Scrivener, Rapid screening tests for supplementary cementitious materials:
593 past and future, Mater. Struct. 49 (2016) 3265–3279. https://doi.org/10.1617/s11527-015-
594 0718-z.
595 [21] V. Kocaba, E. Gallucci, K.L. Scrivener, Methods for determination of degree of reaction of slag in
596 blended cement pastes, Cem. Concr. Res. 42 (2012) 511–525.
597 https://doi.org/10.1016/j.cemconres.2011.11.010.
598 [22] F. Avet, R. Snellings, A. Alujas Diaz, M. Ben Haha, K. Scrivener, Development of a new rapid,
599 relevant and reliable (R3) test method to evaluate the pozzolanic reactivity of calcined kaolinitic
600 clays, Cem. Concr. Res. 85 (2016) 1–11. https://doi.org/10.1016/j.cemconres.2016.02.015.
601 [23] S.T. Erdoğan, T.Ç. Koçak, Influence of slag fineness on the strength and heat evolution of
602 multiple-clinker blended cements, Constr. Build. Mater. 155 (2017) 800–810.
603 https://doi.org/10.1016/j.conbuildmat.2017.08.120.
604 [24] K. Tang, J. Khatib, G. Beattie, Effect of partial replacement of cement with slag on the early-age
605 strength of concrete, Proc. Inst. Civ. Eng. - Struct. Build. 170 (2017) 451–461.
606 https://doi.org/10.1680/jstbu.16.00038.
607 [25] K. Tang, S. Millard, G. Beattie, Early-age heat development in GGBS concrete structures, Proc.
608 Inst. Civ. Eng. - Struct. Build. 168 (2015) 541–553. https://doi.org/10.1680/stbu.14.00089.
609 [26] S. Ramanathan, H. Moon, M. Croly, C.-W. Chung, P. Suraneni, Predicting the degree of reaction
610 of supplementary cementitious materials in cementitious pastes using a pozzolanic test, Constr.
611 Build. Mater. 204 (2019) 621–630. https://doi.org/10.1016/j.conbuildmat.2019.01.173.
612 [27] P. Suraneni, J. Weiss, Examining the pozzolanicity of supplementary cementitious materials
613 using isothermal calorimetry and thermogravimetric analysis, Cem. Concr. Compos. 83 (2017)
614 273–278. https://doi.org/10.1016/j.cemconcomp.2017.07.009.
615 [28] Y. Wang, P. Suraneni, Experimental methods to determine the feasibility of steel slags as
616 supplementary cementitious materials, Constr. Build. Mater. 204 (2019) 458–467.
617 https://doi.org/10.1016/j.conbuildmat.2019.01.196.
618 [29] A. Kashani, J.L. Provis, G.G. Qiao, J.S.J. van Deventer, The interrelationship between surface
619 chemistry and rheology in alkali activated slag paste, Constr. Build. Mater. 65 (2014) 583–591.
620 https://doi.org/10.1016/j.conbuildmat.2014.04.127.
621 [30] P. Drissen, Determination of the glass content in granulated blast furnace slag., Zem. - Kalk -
622 Gips. (1994) 658–661.
623 [31] EN 196-1, Methods of testing cement - Part 1: Determination of strengt, n.d.
624 [32] EN 196-6, Methods of testing cement – Part 6: Determination of fineness, n.d.
625 [33] EN 196-9, Methods of testing cement – Part 9: Heat of hydration, Semi-adiabatic method, n.d.
626 [34] A. Ehrenberg, J. Deubener, N. Pronina, D. Hart, The glass structure of granulated blast furnace
627 slag and its effect on reactivity., in: Proc. 15th Int. Congr. Chem. Cem., Prague, 2019.
628 [35] A. Ehrenberg, Granulated blast furnace slag - From laboratory into practice., in: Beijing, 2015.
629 [36] A. Schöler, B. Lothenbach, F. Winnefeld, M.B. Haha, M. Zajac, H.-M. Ludwig, Early hydration of
630 SCM-blended Portland cements: A pore solution and isothermal calorimetry study, Cem. Concr.
631 Res. 93 (2017) 71–82. https://doi.org/10.1016/j.cemconres.2016.11.013.
632 [37] M. Whittaker, M. Zajac, M. Ben Haha, F. Bullerjahn, L. Black, The role of the alumina content of
633 slag, plus the presence of additional sulfate on the hydration and microstructure of Portland
634 cement-slag blends, Cem. Concr. Res. 66 (2014) 91–101.
635 https://doi.org/10.1016/j.cemconres.2014.07.018.
636 [38] P.Z. Wang, R. Trettin, V. Rudert, T. Spaniol, Influence of Al_2O_3 content on hydraulic reactivity
637 of granulated blast-furnace slag, and the interaction between Al_2O_3 and CaO, Adv. Cem. Res.
638 16 (2004) 1–7. https://doi.org/10.1680/adcr.2004.16.1.1.
639 [39] W. Wassing, Relationship between the chemical reactivity of granulated blastfurnace slags and
640 the mortar standard compressive strength of the blastfurnace cements produced from them,
641 Cem. Int. (2003) 95–109.

642 [40] M. Ben Haha, B. Lothenbach, G. Le Saout, F. Winnefeld, Influence of slag chemistry on the
643 hydration of alkali-activated blast-furnace slag — Part II: Effect of Al2O3, Cem. Concr. Res. 42
644 (2012) 74–83. https://doi.org/10.1016/j.cemconres.2011.08.005.
645 [41] A.R. Sakulich, E. Anderson, C.L. Schauer, M.W. Barsoum, Influence of Si:Al ratio on the
646 microstructural and mechanical properties of a fine-limestone aggregate alkali-activated slag
647 concrete, Mater. Struct. 43 (2010) 1025–1035. https://doi.org/10.1617/s11527-009-9563-2.
648 [42] K. Gong, C.E. White, Impact of chemical variability of ground granulated blast-furnace slag on
649 the phase formation in alkali-activated slag pastes, Cem. Concr. Res. 89 (2016) 310–319.
650 https://doi.org/10.1016/j.cemconres.2016.09.003.
651 [43] B.C. Bunker, Molecular mechanisms for corrosion of silica and silicate glasses, J. Non-Cryst.
652 Solids. 179 (1994) 300–308. https://doi.org/10.1016/0022-3093(94)90708-0.
653 [44] H. Scholze, Glass, Springer New York, New York, NY, 1991. https://doi.org/10.1007/978-1-4613-
654 9069-5.
655 [45] P.J. Schilling, L.G. Butler, A. Roy, H.C. Eaton, 29Si and 27Al MAS-NMR of NaOH-Activated Blast-
656 Furnace Slag, J. Am. Ceram. Soc. 77 (1994) 2363–2368. https://doi.org/10.1111/j.1151-
657 2916.1994.tb04606.x.
658 [46] A. Ehrenberg, Granulated blast furnace slag - State of the art and potentials for the futureCO2
659 emissions and energy consumption of granulated blastfurnace slag, in: Euroslag publication,
660 Madrid, 2011: pp. 277–297.
661 [47] C. Cailleteau, F. Angeli, F. Devreux, S. Gin, J. Jestin, P. Jollivet, O. Spalla, Insight into silicate-glass
662 corrosion mechanisms, Nat. Mater. 7 (2008) 978.
663 [48] R. Snellings, Solution-Controlled Dissolution of Supplementary Cementitious Material Glasses at
664 pH 13: The Effect of Solution Composition on Glass Dissolution Rates, J. Am. Ceram. Soc. 96
665 (2013) 2467–2475. https://doi.org/10.1111/jace.12480.
666 [49] R. Snellings, T. Paulhiac, K. Scrivener, The Effect of Mg on Slag Reactivity in Blended Cements,
667 Waste Biomass Valorization. 5 (2014) 369–383. https://doi.org/10.1007/s12649-013-9273-4.
668 [50] M. Ben Haha, B. Lothenbach, G. Le Saout, F. Winnefeld, Influence of slag chemistry on the
669 hydration of alkali-activated blast-furnace slag — Part I: Effect of MgO, Cem. Concr. Res. 41
670 (2011) 955–963. https://doi.org/10.1016/j.cemconres.2011.05.002.
671 [51] P.T. Durdziński, M. Ben Haha, M. Zajac, K.L. Scrivener, Phase assemblage of composite cements,
672 Cem. Concr. Res. 99 (2017) 172–182. https://doi.org/10.1016/j.cemconres.2017.05.009.
673 [52] P. Termkhajornkit, Q.H. Vu, R. Barbarulo, S. Daronnat, G. Chanvillard, Dependence of
674 compressive strength on phase assemblage in cement pastes: Beyond gel–space ratio —
675 Experimental evidence and micromechanical modeling, Cem. Concr. Res. 56 (2014) 1–11.
676 https://doi.org/10.1016/j.cemconres.2013.10.007.
677 [53] A. Gruskovnjak, B. Lothenbach, L. Holzer, R. Figi, F. Winnefeld, Hydration of alkali-activated slag:
678 comparison with ordinary Portland cement, Adv. Cem. Res. 18 (2006) 119–128.
679 https://doi.org/10.1680/adcr.2006.18.3.119.
680 [54] B. Lothenbach, D.A. Kulik, T. Matschei, M. Balonis, L. Baquerizo, B. Dilnesa, G.D. Miron, R.J.
681 Myers, Cemdata18: A chemical thermodynamic database for hydrated Portland cements and
682 alkali-activated materials, Cem. Concr. Res. 115 (2019) 472–506.
683 https://doi.org/10.1016/j.cemconres.2018.04.018.
684 [55] R. Snellings, X. Li, F. Avet, K. Scrivener, A Rapid, Robust, and Relevant (R3) Reactivity Test for
685 Supplementary Cementitious Materials, ACI Mater. J. 116 (2019).
686 https://doi.org/10.14359/51716719.
687